



HAL
open science

CAR modulates plasma membrane nano-organization and immune signaling downstream of RALF1-FERONIA signaling pathway

Weijun Chen, Huina Zhou, Fan Xu, Meng Yu, Alberto Coego, Lesia Rodriguez, Yuqing Lu, Qijun Xie, Qiong Fu, Jia Chen, et al.

► To cite this version:

Weijun Chen, Huina Zhou, Fan Xu, Meng Yu, Alberto Coego, et al.. CAR modulates plasma membrane nano-organization and immune signaling downstream of RALF1-FERONIA signaling pathway. *New Phytologist*, In press, 10.1111/nph.18687 . hal-03934185

HAL Id: hal-03934185

<https://hal.science/hal-03934185v1>

Submitted on 11 Jan 2023

HAL is a multi-disciplinary open access archive for the deposit and dissemination of scientific research documents, whether they are published or not. The documents may come from teaching and research institutions in France or abroad, or from public or private research centers.

L'archive ouverte pluridisciplinaire **HAL**, est destinée au dépôt et à la diffusion de documents scientifiques de niveau recherche, publiés ou non, émanant des établissements d'enseignement et de recherche français ou étrangers, des laboratoires publics ou privés.

1 **CAR modulates plasma membrane nano-organization and**
2 **immune signaling downstream of RALF1-FERONIA**
3 **signaling pathway**

4 Weijun Chen¹*, Huina Zhou²*, Fan Xu¹, Meng Yu³, Alberto Coego⁴, Lesia Rodriguez⁴, Yuqing
5 Lu³, Qijun Xie¹, Qiong Fu¹, Jia Chen¹, Guoyun Xu², Dousheng Wu¹, Xiushan Li¹, Xiaojuan Li³,
6 Yvon Jaillais⁵, Pedro L. Rodriguez⁴, Sirui Zhu¹, Feng Yu¹¶

7 1. State Key Laboratory of Chemo/Biosensing and Chemometrics, Laboratory of Plant
8 Functional Genomics and Developmental Regulation, College of Biology, Hunan
9 University, Changsha 410082, P. R. China.

10 2. Zhengzhou Tobacco Research Institute, Zhengzhou 450001, P.R. China;

11 3. Beijing Advanced Innovation Center for Tree Breeding by Molecular Design,
12 Beijing Forestry University, Beijing 100083, P. R. China;

13 4. Instituto de Biología Molecular y Celular de Plantas, Consejo Superior de
14 Investigaciones Científicas–Universidad Politécnica de Valencia, ES–46022 Valencia,
15 Spain;

16 5. Laboratoire Reproduction et Développement des Plantes, Université de Lyon, ENS
17 de Lyon, UCB Lyon 1, CNRS, INRAE, F-69342 Lyon, France.

18 Authors for correspondence:

19 Feng Yu

20 Tel: +86 130 5516 4913

21 Email: feng_yu@hnu.edu.cn

22 * W.C. and H.Z. contributed equally to this work.

23 ORCID:

24 Weijun Chen: 0000-0001-7622-2441

25 Feng Yu: 0000-0002-5221-281X

26 Brief heading: The RALF-FER regulates the nano-organization on the membrane via
27 CAR family

28 **Summary**

- 29 ● The receptor-like kinase (RLK) FERONIA (FER) senses peptide ligands in the
30 plasma membrane (PM), modulates plant growth and development, and integrates
31 biotic and abiotic stress signaling for downstream adaptive response. However, the
32 molecular interplay of these diverse processes is largely unknown.
- 33 ● Here, we show that FER, the receptor of Rapid Alkalinization Factor 1 (RALF1),
34 physically interacts with C2 domain ABA-related (CAR) proteins to control the
35 nano-organization of the PM in *Arabidopsis*.
- 36 ● During this process, the RALF1-FER pathway upregulates CAR protein
37 translation, and then more CAR proteins are recruited to the PM. This acts as a
38 rapid feedforward loop that stabilizes the PM liquid-ordered phase. FER interacts
39 with and phosphorylates CARs, thereby reducing their lipid-binding ability, and
40 breaking the feedback regulation at latter time point.
- 41 ● Similar to FER mutant, pentuple *car14569* mutants inhibit flg22-induced FLS2-
42 BAK1 immune complex formation, which depends on the integrity of
43 nanodomains.
- 44 ● Together, we propose that the FER-CAR module controls the formation of the PM
45 nano-organization during RALF signaling through a self-contained amplifying
46 loop including both positive and negative feedbacks.

47 **Key words:** FER, C2 domain ABA-related proteins, lipid-binding, nanodomains,
48 immune complex.

49

50 **Introduction**

51 *Catharanthus roseus* receptor-like kinase 1-like protein (*CrRLK1L*) FERONIA (FER)
52 is a receptor-like kinase with versatile and tissue-specific functions in plant cell growth
53 and survival. FER functions with its ligands, rapid alkalization factors (RALFs, e.g.,
54 RALF1 and RALF23), as a regulator of fertilization (Escobar-Restrepo *et al.*, 2007; Li
55 *et al.*, 2015), cell growth (Guo *et al.*, 2009; Duan *et al.*, 2010; Du *et al.*, 2016; Li *et al.*,
56 2018), hormone signaling (Guo *et al.*, 2009; Duan *et al.*, 2010), stress responses (Chen
57 *et al.*, 2016), immune signaling (Stegmann *et al.*, 2017) and energy and RNA
58 metabolism (Yang *et al.*, 2015; Xu *et al.*, 2019; Wang *et al.*, 2020; Zhu *et al.*, 2020).
59 However, the mechanism through which FER quickly responds to and integrates
60 external signals and transmits them to varied downstream targets remains unknown.
61 Recent report showed that FER acts as a scaffold to regulate the formation of the
62 immune receptor complex (FLS2 and BAK1) to respond to the pathogen-associated
63 molecular pattern (PAMP) flagellin 22 (flg22) in a RALF-dependent manner
64 (Stegmann *et al.*, 2017). Furthermore, the RALF-FER pathway modulates the plasma
65 membrane nanoscale dynamics of immune receptors, via so far elusive mechanisms
66 (Gronnier *et al.*, 2022).

67 Biological membranes are made of a plethora of co-existing nanodomains, which
68 are characterized by their small size (i.e., below 1 μm) and specific proteolipid
69 composition (Spira *et al.*, 2012; Jarsch *et al.*, 2014; Jaillais & Ott, 2020). Such
70 membrane domains are critical in signaling notably because they can locally
71 concentrate proteins, a process known as nanoclustering (Ott, 2017; Jaillais & Ott,
72 2020). By increasing the local concentration of proteins, nanoclustering favors the
73 formation of protein complexes or post-translational modifications, which often act as
74 a trigger to initiate signaling (Jaillais & Ott, 2020; Gronnier *et al.*, 2022). The small
75 protein family flotillin (Flot) and plant-specific remorin protein family are localized in
76 nanodomains in a sterol-dependent manner at the plasma membrane. Multiple
77 evidences suggest that Flots and remorins are not only nanodomain resident proteins
78 but are also crucial to stabilize these nanodomains. Furthermore, they recruit signaling

79 molecules into these structures (Liang *et al.*, 2018; Huang *et al.*, 2019; Jaillais & Ott,
80 2020; Pan *et al.*, 2020). In addition, protein nanoclustering is regulated through the
81 formation of various protein–lipid and protein–protein interactions (Simons & Gerl,
82 2010; Garcia-Parajo *et al.*, 2014; Sezgin *et al.*, 2017; Pan *et al.*, 2020). As such, they
83 act as versatile signaling platforms with very diverse composition in term of lipids and
84 proteins (Burkart & Stahl, 2017; Platre *et al.*, 2019; Jaillais & Ott, 2020). However,
85 how plants regulate the nano-organization of the plasma membrane during signaling is
86 just starting to be elucidated.

87 Accumulating evidence has shown that in plants, nanodomains are important for
88 the cellular response to environmental cues and improving the fitness of plants (Demir
89 *et al.*, 2013; Wang *et al.*, 2015; Bucherl *et al.*, 2017; Huang *et al.*, 2019). Several works
90 have linked the abscisic acid (ABA) response with nanodomain dynamics (Demir *et al.*
91 *et al.*, 2013; Diaz *et al.*, 2016). For example, a 10-member family of lipid-binding C2
92 domain ABA-related proteins (CARs, CAR1 to CAR10) was identified and found to
93 interact with pyrabactin resistance 1 (PYR1)/PYR1-like (PYL)/regulatory components
94 of ABA receptors (RCAR) ABA receptors and to positively regulate ABA signaling
95 (Rodriguez *et al.*, 2014). CARs oligomerize at the PM in a calcium-dependent manner
96 and has been identified in detergent-resistant membranes (DRMs). Furthermore, they
97 induce membrane fusion, possibly by promoting membrane curvature (Martens &
98 McMahon, 2008; Demir *et al.*, 2013; Diaz *et al.*, 2016). However, the upstream
99 regulator(s) that link CARs with the modulation of the PM landscape is still unknown.
100 Herein, we propose a working model in which FER works together with lipid-binding
101 CAR proteins to regulate the partitioning of liquid-ordered and liquid-disordered phases
102 of the plasma membrane. In this scenario, activation of FER by RALF1 triggered the
103 accumulation and phosphorylation of downstream CAR proteins, thereby modulating
104 the plasma membrane nano-organization in a dynamic manner.

105 **Materials and Methods**

106 **Plant Material and Growth Conditions.**

107 *Arabidopsis* (Col-0) was used as the wild-type (WT). The following transgenic and
108 mutant lines were used in this study: *CAR1-Myc*, *CAR4-Myc*, *CAR5-Myc*, *CAR6-Myc*,
109 *CAR9-Myc*, *CAR10-Myc*, *CAR9-Myc/fer-4*, *YFP-CAR9*, *YFP-CAR9/fer-4*, *CAR9^{3M}-*
110 *YFP*, *CAR9^{3M}-YFP/fer-4* and *car59*, *car145*, *car459*, *car149*, *car159*, *car1459*,
111 *car14569-Δ1*, *car14569-Δ4*, *car14569-Δ10*, *car14569-Δ20*.

112 *Arabidopsis thaliana* seeds were first surface sterilized by 75 % (v/v) ethanol. After
113 stigmatization at 4 °C for 3 d, seeds were growing on 1/2 MS with 0.8 % sucrose and
114 1.0 % Phytagel (Sigma-Aldrich) at 22 °C in a 16-h light/8-h dark condition for
115 subsequent analysis. Details of this information are described in [Methods S1](#).

116 **Yeast Two-Hybrid (Y2H) Assay.**

117 Y2H assays were performed as previously described (Du *et al.*, 2016). Briefly, the
118 cytoplasm domain of *CrRLK1L* family members (AT3G51550, FER, 469–896 amino
119 acids; AT2G39360, CVY1, 429–815 amino acids; AT5G38990, MDS1, 462–880
120 amino acids; AT5G39020, MDS3, 459–813 amino acids; AT1G30570, HERK2, 451–
121 849 amino acids), and two RLKs (AT5G46330, FLS2, 870–1155 amino acids;
122 AT4G39400, BRI1, 814–1196 amino acids) were fused in-frame with the GAL4
123 DNA-binding domain of the bait vector pGBKT7. The CDS of *CARs* were fused with
124 the GAL4 DNA-activating domain of the prey vector pGADT7 (AD-CAR). Distinct
125 plasmid pairs were transformed into yeast AH109 cells. The diluted transformants were
126 plated onto synthetic dropout medium lacking tryptophan/leucine (SD/-Trp-Leu+His)
127 and synthetic dropout medium lacking tryptophan/leucine/histidine (SD/-Trp-Leu-
128 His) but supplemented with 20 mM 3-amino-1,2,4-triazole (3-AT) for 4 days to test
129 the interaction.

130 **Co-Immunoprecipitation (Co-IP) Assay.**

131 Co-IP was performed as previously described with some modifications (Li *et al.*, 2018).
132 Seven-day-old seedlings *35S::CARs-Myc* (about 0.5 g) were ground to a fine powder
133 in liquid nitrogen and solubilized with 500 μL TBST buffer [50 mM Tris-HCl (pH 7.5),
134 150 mM NaCl, 5 mM MgCl₂, 1 mM EDTA, 1 % Triton X-100] containing 1 × protease

135 inhibitor cocktail (78430, Thermo Fisher Scientific) and 1 × phosphatase inhibitor
136 (78420, Thermo Fisher Scientific) and spun for 1 hour at 4 °C. The extracts were
137 centrifuged at 16,000 g at 4 °C for 10 min, and 500 µL supernatant was transferred to
138 incubate with prepared 20 µL Anti-Myc magnetic beads (B26301) overnight at 4 °C,
139 and 100 µL supernatant was used as input. Then, the beads were washed 3 times with
140 the washing buffer [50 mM Tris-HCl (pH 7.5), 150 mM NaCl, 0.1 % Triton X-100]
141 containing 1 × protease inhibitor cocktail and eluted with elution buffer (0.2 M Glycine,
142 1 % Triton X-100, 1 mM EDTA, pH 2.5). And proteins were run on a 10 % SDS-
143 PAGE gel and analyzed by anti-FER (Du *et al.*, 2016; Li *et al.*, 2018) and anti-Myc
144 (CST, 2276S) antibody.

145 ***In vitro* Phosphorylation Assay.**

146 The phosphorylation and dephosphorylation assays were described as previously (Du,
147 *et al.*, 2016). GST-CAR9, GST-CAR5, FER-CD-His and FER^{K565R}-CD-His (kinase
148 dead form) were purified for phosphorylation assay *in vitro*.

149 The ABA-induced phosphorylation co-expression system was described
150 previously (Li *et al.*, 2018). Vectors of pACYC-PYL1-FER (S-tag), pACYC-PYL1-
151 FER^{K565R} (S-tag), and pRSF-ABI1-CAR9 (His-tag) were constructed and co-
152 transformed into one BL21 (DE3) *E. coli* strain. His-CAR proteins were purified and
153 then subjected to liquid chromatography-tandem mass spectrometry (LC-MS/MS).
154 Details of this method are described in [Methods S1](#).

155 ***In vivo* Phosphorylation Assay.**

156 Phos-tag assay was performed as described previously (Chen *et al.*, 2018). Seven-day-
157 old *CAR-Myc* seedlings were used to analyze phosphorylated band *in vivo*. For
158 phosphorylation sites detecting *in vivo*, *CAR-Myc* was enriched by immunoprecipitate.
159 The *CAR-Myc* bands digested and analyzed by LC-MS/MS as described previously.
160 Details of this method are described in [Methods S1](#).

161 **Pan-anti-CARs Antibody Production.**

162 Antibody production was performed as previous study (Li *et al.*, 2018). This antibody
163 is raised by using full-length CAR9 expressed and purified from *E.coli* BL21. A 1-
164 month-old ICR mouse (SLAC laboratory animal) was injected with 50 µg GST-CAR9
165 protein emulsified with Complete Freund's adjuvant (F5881, Sigma-Aldrich). Two
166 weeks later, 50 µg GST-CAR9 protein emulsified with Incomplete Freund's adjuvant
167 (F5506, Sigma-Aldrich) was injected into the ICR mouse and then once again in the
168 next week. The serum of the immunized mouse was obtained as antibody for
169 immunoblot detection. We tested the antibody in WT, *car9*, *car459* and *car14569*
170 mutant lines by an immunoblot. Because of ten CAR family members share common
171 motif and sequence, we still detected homologs in CAR9 signal mutants using this
172 antibody, but this interacted band will be sharply reduced when using in CARs multiple
173 mutants. Thus, we named this antibody as pan-anti-CARs antibody.

174 **Lipid Binding Assay.**

175 Phospholipid binding to proteins was assessed as described (Rodriguez *et al.*, 2014).
176 Briefly, phosphatidylserine (PS): phosphatidylcholine (PC) (25:75) was prepared in
177 chloroform and dried to obtain a thin layer under a stream of nitrogen. The dried lipids
178 were resuspended in buffer A (100 mM NaCl, 50 mM HEPES, pH 6.8) and mixed by
179 vortexing for 20 min. Large multilamellar vesicles were obtained by centrifugation at
180 16,000 g for 20 min. Resuspended the vesicles in 1 mL of buffer A with multiple
181 concentrations of free Ca²⁺ and stored at 4 °C. The vesicles (about 100 µg of
182 phospholipids) were mixed with the different forms of GST-CAR9 (5 µg). The mixture
183 was incubated with or without 1 mM Ca²⁺ via gentle shaking (250 rpm) for 30 min at
184 room temperature. The vesicles and the bound proteins were pelleted by centrifugation
185 at 12,000 g at 4 °C for 10 min and washed twice with 0.5 mL of buffer A. Samples were
186 boiled with 1 × protein loading buffer for 10 min and separated by 10 % SDS-PAGE.
187 Proteins were revealed by using anti-GST antibody.

188 **Variable-Angle Total Internal Reflection Fluorescence Microscopy (VA-TIRFM)** 189 **Imaging.**

190 VA-TIRFM was performed as previously described (Li et al., 2012). For observation,
191 seedlings were softly transferred onto a glass slide and soaked with liquid 1/2 MS, then
192 covered with a coverslip. A custom-built VA-TIRFM based on an Olympus IX-71
193 microscope equipped with a total internal reflective fluorescence illuminator and a 100
194 × oil-immersion objective (numerical aperture of 1.45, Olympus) was used here. The
195 473 nm laser line from a diode laser was used to excite GFP. The emission fluorescence
196 signals were detected with a back-illuminated EM-CCD camera (ANDOR iXon
197 DV8897D-CS0-VP; And / or Technology, Belfast, UK) after filtering with band-pass
198 filters. The gain of the EMCCD camera was set to 300 throughout all single-molecule
199 imaging experiments; the setting was in the linear dynamic range of the EMCCD
200 camera. Images were acquired with an exposure time and analyzed with Image J.

201 **Polysome Profiling Assay and Real-Time qPCR.**

202 *Arabidopsis* polysomes profiling assay was performed as described (Missra & Von
203 Arnim, 2014; Zhu *et al.*, 2020). Briefly, 7-day-old seedlings (about 0.5 g) were treated
204 with RALF1 (1 μM) for 10 min and then ground in liquid nitrogen followed by
205 resuspension in polysome extraction buffer. Supernatant was loaded onto a 15 %-60 %
206 sucrose gradient and spun in a Beckman SW 32 Ti rotor at 170,000 g for 4 h at 4 °C.
207 We manually collected 11 fractions. Then, isolated the RNA from the last four fractions
208 by RNAiso plus (Takara) kit. RT-qPCR analysis was used to quantify the total target
209 relative transcript content in the input and the relative content of target transcripts
210 associated with heavier polysomes in the bottom four fractions. Primers for RT-qPCR
211 is shown in [Table S1](#). *ACTIN* as a reference gene to detect the RNA levels of CARs.

212 **Di-4-ANEPPDHQ Lipid Staining.**

213 For di-4-ANEPPDHQ lipid staining, four-day-old seedlings are collected for each
214 genotype. 5 μM (work concentration) di-4-ANEPPDHQ was added in liquid 1/2 MS
215 medium for staining. Quantification of lipid polarity in root cell has been described
216 previously (Huang et al., 2019; Owen et al., 2011). Details of this method are described in
217 [Methods S1](#).

218 **ROS Burst Assay.**

219 The flg22-induced ROS burst measurement assay was performed as previously
220 described (Stegmann *et al.*, 2017). Four-week-old *Arabidopsis* rosette leaves were
221 used for ROS dynamic determination. ROS fluorescent probe H2DCF-DA staining
222 (James *et al.*, 2015) 6-day-old seedlings were treated with the liquid 1/2 MS medium
223 containing 10 μ M H2DCF-DA. Fluorescence was monitored with a confocal
224 microscope using an excitation wavelength of 488 nm. Details of this method are
225 described in [Methods S1](#).

226 ***Pto* DC3000 infection assay.**

227 For *Pto* DC3000 infection assay (Stegmann *et al.*, 2017), *Pseudomonas syringae pv.*
228 *Tomato (Pto)* DC3000 strains were grown overnight in King's B medium (10 g/L
229 proteose peptone, 1.5 g/L anhydrous K₂HPO₄, 5 g/L MgSO₄) with shaking at 28°C.
230 Bacteria were collected from centrifuge tube and resuspended in water containing
231 0.02% Silwet L77 (Sigma Aldrich) to an OD₆₀₀ = 0.2 (10⁸ colony forming units per
232 mL). This bacterial suspension was sprayed on 4-week-old plants, which were covered
233 with vented lids for 3 days. Three leaf discs per sample from different plants were
234 collected in different microfuge tubes and ground with a drill-adapted pestle. Serial
235 dilutions were plated on LB agar and colonies were counted 2 days later.

236 **Statistical Analysis.**

237 Software SPSS Statistics 17.0 was used. Data are shown as mean \pm s.d.; * $p < 0.05$, **
238 $p < 0.01$, *** $p < 0.001$; n.s., not significant. One-way ANOVA with Tukey's test were
239 used as mention in figure note.

240 **Results**

241 **Lipid-binding CAR proteins physically interact with the receptor kinase FER at**
242 **the PM**

243 FER is involved in response to multiple extracellular signals (Zhu *et al.*, 2021), and
244 controls the dynamics of FLS2 and BAK1 in response to RALF signal (Gronnier *et al.*,

245 2022). To understand the functions of FER, we performed a yeast two-hybrid (Y2H)
246 screen using the cytoplasmic domain of FER (FER-CD, 469–896 amino acids, aa) as
247 bait (Du *et al.*, 2016). Among the interacting proteins, we found *CAR9*, which belongs
248 to a 10-member family of lipid-binding C2 domain ABA-related proteins (Rodriguez
249 *et al.*, 2014; Diaz *et al.*, 2016; Qin *et al.*, 2019). We cloned the full-length genes for the
250 ten *CAR* family members (*CAR1* – *CAR10*) and found that *CAR1*, *CAR4*, *CAR5*, *CAR6*,
251 *CAR9* and *CAR10* were able to directly interact with FER-CD in Y2H assays (Fig. 1a
252 and Fig. S1a). Next, glutathione S-transferase (GST) pull-down assays further
253 confirmed the interaction between CARs (GST-tagged *CAR1*, *CAR4*, *CAR5*, *CAR6*,
254 *CAR9* and *CAR10*) and His-tagged FER-CD (Fig. 1b and Fig. S1b). Furthermore,
255 bimolecular fluorescence complementation (BiFC) assays were used to test the
256 interaction between CARs and FER in *Arabidopsis* protoplasts. The results showed that
257 *CAR1*, *CAR4*, *CAR5*, *CAR6*, *CAR9*, and *CAR10* interacted with FER at the PM (the
258 protein-protein interaction caused green fluorescence, which overlapped with FM4-64
259 PM red fluorescence) (Fig. 1c). We next performed coimmunoprecipitation (co-IP)
260 assays and confirmed the interaction between Myc-tagged CAR proteins (i.e., *CAR1*,
261 *CAR4*, *CAR5*, *CAR6*, *CAR9*, *CAR10*) and FER *in vivo* (Fig. 1d and Fig. S1c). To
262 further verify the specificity of the interaction between CARs and FER, we cloned the
263 cytoplasmic domains of five *CrRLK1L* family members (*CVY1*, AT2G39360; *BUPS1*,
264 AT4G39110; *MDS1*, AT5G38990; *MDS3*, AT5G39020; *HERK2*, AT1G30570) and
265 two LRR-RLKs (*FLS2* and *BRI1*) and further analyzed their interaction with *CAR9*.
266 The results of the Y2H assays showed that *CAR9* interacted specifically with FER and
267 *BUPS1*, but not with the other six kinase domains (Fig. S1d). We also performed co-
268 IP assays between Y2H noninteracting CARs (e.g., *CAR3* and *CAR7*) and FER (Fig.
269 S1e). The results revealed no interaction of *CAR3* and *CAR7* with FER *in vivo*, which
270 indicates that the interaction between certain CARs and FER is specific. Taken
271 together, these data suggest that FER physically interacts with a subset of CAR proteins
272 at the PM.

273 **FER phosphorylates CARs, which further regulates the interaction of CARs with**
274 **lipids**

275 To evaluate whether CARs could be substrates of FER, we first tested CAR5 and CAR9
276 by using phosphorylation assays *in vitro*. The results showed that recombinant FER–
277 CD induced a higher phosphorylation level in the CAR5 and CAR9 proteins (Fig. 2a).
278 To further assess whether the phosphorylation levels of these two proteins were
279 enhanced by RALF1 *in vivo*, Phos–Tag–PAGE analysis (Chen *et al.*, 2018) was used
280 to detect phosphorylated forms of CAR5 and CAR9 (thereafter referred to as pCAR5
281 and pCAR9) in plants expressing Myc-tagged CARs with or without RALF1 treatment
282 (Fig. 2b). Notably, RALF1 treatment altered CAR protein abundance in *Arabidopsis*
283 (detailed description in Fig. 3); thus, we adjusted the total protein levels (including
284 those of phosphorylated and dephosphorylated proteins). We found a slow running
285 form of CAR5 and CAR9, that was strongly reduced by alkaline phosphatase treatment
286 (CIP), suggesting that they corresponded to pCAR5 and pCAR9. RALF1 treatment (1
287 μM , 30 min) increased the phosphorylation levels of both CAR5 and CAR9 *in vivo*
288 (Fig. 2b). Time series analysis indicated that the phosphorylation level of CAR5 and
289 CAR9 increased at 20 min and 40 min post RALF1 treatment (protein abundance was
290 adjusted prior to western blotting) in the WT background, but not in *fer-4* (Fig. S2).
291 Together, our results indicate that RALF1-mediated CAR phosphorylation is dependent
292 on FER.

293 We further identified the FER-mediated phosphorylation sites of CAR5 and CAR9
294 using a previously developed ABA-induced co-expression system (Li *et al.*, 2018). A
295 kinase-dead mutant of FER–CD (Lys at 565 was mutated into Arg, FER–CD^{K565R}) was
296 used as a negative control (Escobar-Restrepo *et al.*, 2007). Electrospray ionization
297 (ESI) mass spectrometry (ESI-MS) analysis indicated that after ABA induction, FER
298 phosphorylated CAR5 at Ser61, Ser62, and Tyr65 (Fig. S3a–S3c). Of note, in the same
299 assay, Thr26, Ser27, and Tyr30 were phosphorylated in CAR9 (Fig. S3d and S3e),
300 which are the equivalent phosphorylated residues in CAR5 (Fig. S4a), reinforcing the
301 idea that those phosphorylation sites could be physiologically relevant. Moreover, 2 out
302 of 3 sites were further verified *in vivo* by label-free quantitative MS, and we found that

303 RALF1 enhanced the CAR5 phosphorylation level at Ser62 and Tyr65 compared with
304 mock-treated plants (Fig. 2c and Fig. S3f). To confirm that GST-CAR5 and GST-
305 CAR9 were phosphorylated by FER-CD on these three residues, we next mutated the
306 phosphorylated Serine/threonine into alanine (Ala) and tyrosine into phenylalanine
307 (Phe) (GST-CAR5^{3M/9^{3M}}) (Li *et al.*, 2018; Zhou *et al.*, 2018). GST-CAR5^{3M} and
308 GST-CAR9^{3M} remained unphosphorylated by FER in vitro (Fig. 2d). These data
309 suggest that RALF1 promotes the FER-mediated phosphorylation of CAR5 and CAR9
310 at those specific sites.

311 We found that after adding ATP into the reaction system to activate the
312 phosphorylation activity of FER, the intensity of the interaction between the FER and
313 CAR9 was significantly attenuated. However, the intensity of CAR9^{3M} interaction with
314 FER was no longer significantly regulated by phosphorylation (Fig. 2e and S4b). We
315 then tested the effect of a CAR9 phosphorylation mimic on this interaction. We mutated
316 three phosphorylation sites of CAR9 (Thr26, Ser27, Tyr30) to Asp (D) (GST-CAR9^{3D})
317 to test how the mutant residues affected the FER-CAR9 association. Compared with
318 wild-type CAR9, GST-CAR9^{3D} exhibited a lower association with FER-CD (41% ±
319 5.2% weakened) and FER^{K565R}-CD (42% ± 7.4% weakened) (Fig. 2f). These results
320 indicated that the phosphorylation of CAR9 reduces its affinity toward FER.

321 CARs have been found located in nanodomains and directly interact with
322 negatively-charged phospholipid to promote membrane fusion (Martens *et al.*, 2007;
323 Demir *et al.*, 2013; Rodriguez *et al.*, 2014). To test whether FER regulates the
324 interaction between CAR and lipids via phosphorylation, we investigated the lipid-
325 binding ability of CAR under phosphorylated and non-phosphorylated states
326 (Rodriguez *et al.*, 2014). Since the Ca²⁺-dependent anionic phospholipid binding is a
327 hallmark of many C2 domains (Rodriguez *et al.*, 2014), we confirmed that several CAR
328 proteins (CAR5, 6, 9, and 10) directly interact with negatively charged phospholipid
329 vesicles [25:75 (w/w) mixture of phosphatidylserine: phosphatidylcholine] in the
330 presence of free Ca²⁺ (Fig. S5a and S5b). Furthermore, we compared the effect of wild-
331 type FER and kinase-dead FER (FER^{K565R}) on CAR5 and CAR9 in lipid

332 cosedimentation assays and found that phosphorylated CAR5 and CAR9 (coincubated
333 with FER-CD and ATP) had a weakened capacity to interact with anionic
334 phospholipids (Fig. 2g and 2h). Furthermore, comparison of the lipid binding ability of
335 two mutant forms of CAR9 protein (GST-CAR9^{3M} and GST-CAR9^{3D}) toward
336 negatively-charged phospholipid vesicles revealed that CAR9^{3M} exhibited a similar
337 association with vesicles than the wild-type CAR9, whereas CAR9^{3D} showed weaker
338 binding ability (Fig. 2i).

339 A previous study used negative stain transmission electron microscopy (TEM) to
340 show that CAR can interact with negatively-charged phospholipid vesicles and further
341 induce membrane curvature (Diaz *et al.*, 2016). To answer whether FER could
342 modulate membrane curvature via regulating the affinity between CARs and anionic
343 phospholipids, we tested the effect of CAR9 phosphorylation on its membrane bending
344 activity (Fig. S5c-S5j). Addition of free Ca²⁺ and CAR9 to negatively-charged
345 phospholipid vesicles induced strong tubulation of the liposomes (Fig. S5g and S5j).
346 GST-CAR9^{3M} induced strong tubulation of liposomes (Fig. S5h and S5j), whereas
347 GST-CAR9^{3D} significantly reduced tubulation (Fig. S5i and S5j). Thus our data
348 indicate that FER phosphorylates CARs at specific sites, which further fine-tunes the
349 association of FER and CARs. Moreover, in vitro, CAR9-induced membrane curvature
350 is finely regulated by the kinase activity of FER.

351

352 **RALF1-FER regulates CAR nanoclustering via promoting CAR protein** 353 **translation**

354 From above, several evidences implied that CAR proteins localization in nanodomains
355 may be regulated by FER. To investigate how RALF1-FER affects the CAR
356 nanoclusters on the PM, time-lapse images were collected with a variable-angle total
357 internal reflection fluorescence (VA-TIRF) microscope for 4-day-old *YFP-CAR9* root
358 cells followed by single-particle-tracking method (Pan *et al.*, 2020). Treatment with 1
359 μ M RALF1 resulted in an increase in the density of YFP-CAR9 particles (Fig. 3a and

360 Fig. 3b), which suggests that more CAR proteins are localized to the membrane and
361 recruited into CAR-associated nanoclusters. Furthermore, similar to the treatment with
362 sterol-depleting agent methyl- β -cyclodextrin (M β CD), density of YFP-CAR9 particles
363 in *fer-4* background was significantly decreased (Fig. 3a and Fig. 3b). Evidence shows
364 that many proteins on the PM are not uniformly mixed with membrane lipids via free
365 diffusion-based equilibrium, but laterally segregated into nanodomains with a limited
366 diffusion and specific lipids (Jaillais & Ott, 2020; Pan *et al.*, 2020). Treatment with
367 RALF1 induced a slower diffusion coefficient of YFP-CAR9-containing nanoclusters
368 (Fig. 3c). By contrast, YFP-CAR9 nanodomains showed a higher diffusion coefficient
369 after treatment with M β CD, or in the *fer-4* background (Fig. 3c). Next, we tested the
370 dynamic changes in membrane order induced by RALF1 treatment. We found that
371 RALF1 promotes the liquid-ordered phase of the plasma membrane in the first 10 min
372 of the treatment. Intriguingly, with the prolongation of RALF1 treatment, the
373 proportion of lipid ordered phase maintained a dynamic equilibrium (Fig. S6a and S6b),
374 which showed a similar trend with CAR phosphorylation (Fig. S2). Then, we expressed
375 the YFP-CAR9^{3D} and YFP-CAR9^{3M} in WT background. VA-TIRFM analysis showed
376 that YFP-CAR9^{3D} particles resulted in a shorter dwell time at the plasma membrane
377 than YFP-CAR9 and YFP-CAR9^{3M} (Fig. S6c-S6f). These results suggest that RALF1
378 promotes the formation of CAR9 nanoclusters, possibly by recruiting more CAR
379 proteins into nanodomains. Subsequently, FER negatively regulates the dwell time of
380 CAR proteins in nanodomains via directly interacting with and phosphorylating CAR
381 on the membrane, thus forming a feedback loop.

382 A recent study showed that the RALF1-FER promotes protein synthesis through
383 facilitating translation initiation (Zhu *et al.*, 2020); thus, we hypothesized that RALF1-
384 FER facilitates the formation of CAR-containing nanoclusters via promoting their
385 protein synthesis. To test this hypothesis, we investigated the protein accumulation of
386 CARs by using a pan-anti-CARs antibody (see Methods for details) (Fig. S7a).
387 Western blots showed that that RALF1 triggered the rapid accumulation of CAR
388 proteins in WT, but not in the *fer-4* mutant (Fig. 3d). The RALF1-triggered rapid
389 accumulation of CAR1, 4, 5, 6, 9, and 10 proteins was further confirmed in transgenic

390 lines expressing Myc-tagged CAR proteins (Fig. S7b). We also tested the accumulation
391 of three CAR proteins (i.e., CAR2, CAR3 and CAR7) which have no interaction with
392 FER, and found that RALF1 induced protein accumulation of CAR2, but not CAR3 or
393 CAR7 (Fig. S7c). This may imply that the RALF peptides and FER modulate CAR
394 protein accumulation in a sophisticated way. In addition, treatment with ABA (10 μ M)
395 did not induce the accumulation of CAR9 (Fig. S7d). We then tested whether the
396 RALF1-FER complex modulated *CAR* mRNA translation using polysome profiling
397 analysis (Zhu *et al.*, 2020). RALF1 promoted the mRNA translation of *CAR1*, 4, 5, 6,
398 9, and 10 in WT (Fig. 3e). However, the *fer-4* mutant blocked RALF1-triggered *CAR1*,
399 4, 5, 6, 9, and 10 mRNA translation (Fig. 3f), confirming that RALF1 upregulated the
400 protein synthesis of CAR via FER. Together, these results suggest that RALF1-FER
401 promotes CAR proteins synthesis by facilitating their translation rate. Accumulated
402 CAR proteins are then recruited to the PM, facilitating the formation of nanoclusters.

403 **CAR proteins are required for RALF1-FER-induced lipid ordering**

404 We next investigated whether RALF1-FER affects the nano-organizations of the PM.
405 Lipid membranes lateral segregate into domains that are in a liquid-disordered (Ld) or
406 liquid-ordered (Lo) phase. The Lo phase is enriched in sterols and glycosphingolipids,
407 which are segregated into a more tightly packed phase (Huang *et al.*, 2019; Jaillais &
408 Ott, 2020). To test whether RALF1-FER directly impact the lipid order in biological
409 membranes, we took advantage of the lipid order-sensitive probe di-4-ANEPPDHQ
410 (Owen *et al.*, 2011; Huang *et al.*, 2019; Pan *et al.*, 2020). When di-4-ANEPPDHQ
411 molecules detect lipid phases with different dipole potentials in the cell membrane,
412 there is a large shift in the peak emission wavelength of the dye from 630 nm in the Ld
413 phase to 570 nm in the Lo phase (Fig. S8A). The Lo phase shows a higher generalized
414 polarization (GP) value (increased green fluorescence compared with red) (Huang *et*
415 *al.*, 2019). Taking advantage of this assay, we found that *fer-4* had a lower GP value
416 than the WT, indicating a general decreased level of ordered lipids in the PM (Fig 4a
417 and 4b). Furthermore, treatment with 1 μ M RALF1 promoted the higher GP value in
418 WT, but not in *fer-4* (Fig 4a and 4b). To validate this RALF1 effect, we examined lipid

419 order in the presence of M β CD, which depletes sterols, reducing the Lo phase (Huang
420 *et al.*, 2019). As expected, the GP value strongly decreased after M β CD treatment in
421 WT (Fig. 4c and 4d), and the effect of RALF1 on Lo phase formation was also
422 suppressed by M β CD treatments (Fig. 4c and 4d).

423 Next, we used the Di-4-ANEPPDHQ stain assay to analyze lipid order before and
424 after RALF1 treatment in high-order CAR mutants. A *car59* double mutant did not
425 show obvious changes in lipid order, and the sensitivity of *car59* to RALF1-triggered
426 higher lipid order formation, was similar to WT using 1 μ M RALF1 (Fig. 4e and 4f).
427 We thus generated higher-order CAR mutants, and observed a significant difference in
428 lipid order between *car459* or *car1459* mutants and WT (Fig. 4e and 4f). Notably, lipid
429 order of *car1459* showed lower sensitivity to RALF1 than WT (Fig. 4f). Next, we
430 generated 4 independent *car14569* pentuple mutants by designing a CRISPR-Cas9-
431 mediated CAR6 knockout in *car1459* background, termed as *car14569*- Δ 1, *car14569*-
432 Δ 4, *car14569*- Δ 10, *car14569*- Δ 20 (all of them harbor out-of-frame deletions in *CAR6*,
433 details in materials and methods). Di-4-ANEPPDHQ stain revealed that the pentuple
434 mutant *car14569*- Δ 20 strongly attenuated the lipid order of the PM, and as expected,
435 *car14569*- Δ 20 displayed insensitivity to RALF1-induced lipid order formation (Fig.
436 4e and 4f). We also analyzed lipid ordering in WT, *fer-4*, and CAR9-Myc/*fer-4* plants.
437 When overexpressed in the *fer-4* background, CAR9-Myc partly rescued the lipid
438 order defects of *fer-4* (Fig. S8b and S8c).

439 To confirm that RALF1 promotion of Lo formation is dependent on the rapid
440 accumulation of CAR proteins, we tested lipid ordering phase in the *eif4e1 eif(iso)4e*
441 translation initiation factor double mutant (Zhu *et al.*, 2020). This double mutant is
442 impacted in the rapid translation of downstream proteins regulated by FER, including
443 CAR proteins. The results showed that membranes exhibited low lipid ordering and no
444 longer responded to RALF1 regulation in the *eif4e1 eif(iso)4e* background (Fig. S9a,
445 S9b, S9e and S9f). Moreover, pretreatment with the translation inhibitor cycloheximide
446 (CHX) before RALF1 indicated that RALF1 no longer promotes Lo phase formation
447 once the rapid accumulation of CAR proteins was prevented by CHX treatment (Fig.
448 S9c, S9d, S9e and S9f). Taken together, these data indicate that rapid accumulation of

449 CAR proteins is necessary for RALF1-FER-triggered higher lipid ordering phase
450 formation, and this process is regulated by multiple CAR family members.

451 **RALF1-FER-CARs regulates plant immunity by regulating FLS2_BAK1**
452 **association.**

453 A recent study found RALF-FER regulates the assembly of immune receptor kinases
454 complexes via modulating plasma membrane nanoscale landscape (Gronnier *et al.*,
455 2022). Our data described above show that the receptor kinase FER regulates membrane
456 biophysical properties through CAR proteins in response to the RALF1 peptide. Thus,
457 we wondered whether the RALF1-FER-CAR axis, through the promotion of an ordered
458 lipid phase of the PM, is able to modulate the assembly of immune complexes. ROS
459 burst results showed that when M β CD pretreatment was used to deplete sterols from
460 membranes, the response of plants to RALF and flg22 peptides was significantly
461 weakened (Fig. S10a-S10d). Next, we examined the flg22-induced association between
462 immune receptor kinases FLS2 and its co-receptor BAK1 in *car14569- Δ 20* pentuple
463 mutant. In agreement with previous results (Stegmann *et al.*, 2017), we confirmed that
464 the association of FLS2 and BAK1 was severely weakened in *fer-4* compared to WT
465 after flg22 treatment (85% \pm 4.5% reduction of the Co-IP signal) (Fig. 5a and 5c). The
466 Co-IP assay of FLS2-BAK1 was also weakened in *car14569- Δ 20* after flg22 treatment
467 compared to WT (25% \pm 6.2% reduction). This effect was weaker than in *fer-4*,
468 possibly because of residual CAR activity remaining in the pentuple *car* mutant (Fig.
469 5b and 5c). As RALF23 does (Stegmann *et al.*, 2017), the activation of FER by RALF1
470 inhibited FLS2 and BAK1 interaction induced by flg22 in the WT (48% \pm 8.2%
471 reduction) (Fig. 5a and 5c). In this co-signaling context, in the absence of FER (*fer-4*),
472 RALF1 had no effect, whereas the residual CAR activity of the *car14569- Δ 20* mutant
473 still mediated the RALF1 inhibitory effect on FLS2-BAK1 interaction, although less
474 efficiently than in WT (compare WT lanes +flg22/+flg22+RALF1 with corresponding
475 *car14569- Δ 20* lanes) (Fig. 5b and 5c). To answer whether CARs can directly respond
476 to flg22-triggered plant immunity, firstly, we tested the accumulation of CAR proteins
477 after flg22 treatment, and the result showed that CAR proteins abundance was

478 insensitive to flg22 treatment (Fig. S11a). Then, VA-TIRFM analysis of CAR9
479 nanoclustering on the membrane found that flg22 treatment has no significant effect on
480 CAR9 nanoclustering in WT and *fer-4* background (Fig. S11b and S11c). This suggests
481 that flg22 is not directly involved in the regulation of CAR proteins' nanoclustering.

482 To further examine the biological relevance of CARs' function in the RALF-FER
483 pathway, we analyzed CARs' role in RALF1-FER-mediated immunity response.
484 Flg22-induced ROS production was attenuated in pentuple CAR mutants (Fig. 5d, 5e,
485 S12a, and S12b). The pentuple CAR mutants were more susceptible to the
486 *Pseudomonas syringae pv. tomato (Pto)* DC3000, albeit not to the same extent as *fer-4*
487 (Fig. 5f and 5g). In addition, overexpression of wild-type CAR9 in *fer-4* partially
488 restored the immunodeficient phenotype of *fer-4*, but not CAR9^{3M} (Fig. 5f and 5g).
489 Taken together, the RALF1-FER-CAR module is necessary for the regulation of plant
490 immunity, which depends on the assembly of immune receptor complexes in specific
491 membrane nanodomains.

492 In addition, FER has also been reported to be involved in cell growth, hormone
493 signaling, stress responses (Zhu *et al.*, 2021). Notably, by comparing the phenotype of
494 *fer-4* and multiple CAR mutants, we observed that *fer-4* and CAR mutants showed a
495 similar defect in root hair and epidermal cell growth and overexpression of CAR9 in
496 *fer-4* background was also able to partly rescue the root hair growth defect (Fig. S13a-
497 S13d). Furthermore, analysis of the effects of temperature stresses on *fer-4* and
498 *car14569-Δ20*, showed hypersensitive phenotypes to temperature stress in both
499 mutants (Fig. S13e-S13h). Together, this set of results shows that RALF1 induces the
500 formation of ordered lipid nanodomains through CAR proteins, and is crucial for FER
501 to regulate multiple signaling pathways.

502 Discussion

503 The molecular mechanisms through which eukaryotic cells modulate their PM
504 landscape via activating receptor kinases in response to external signals remain unclear
505 (Jaillais & Ott, 2020). Our study reveals that FER regulates the general lipid order of
506 the membrane in response to RALFs extracellular peptides. Proteins with C2 domains

507 are involved in protein transport and membrane fusion via interacting with negatively
508 charged phospholipid (Martens *et al.*, 2007; Martens & McMahon, 2008; Rodriguez *et*
509 *al.*, 2014). A lipid binding protein family with C2 domain, CAR, lipid ordering via their
510 rapid accumulation in response to RALF1 (within 10 min after RALF1 treatment).
511 Multiple CAR proteins interact with FER at the PM and are phosphorylated by the
512 kinase (20 min after RALF1 treatment), weakening the ability of CARs to interact with
513 lipids thus form a negatively feedback. The higher ordered lipids, which are particularly
514 induced by RALF1-FER-CAR axis, might be involved in signaling multiple rapid
515 responses, including immunity (Fig. 6).

516 An early and rapid response to the RALF1 peptide is the FER-triggered Ca^{2+} wave
517 (Ngo *et al.*, 2014). Thus, it is reasonable to assume that the RALF1-FER-induced Ca^{2+}
518 wave can further enhance the PM location of CAR proteins (Rodriguez *et al.*, 2014). In
519 agreement with previous studies, we found that Ca^{2+} upregulates the lipid binding and
520 membrane curvature ability of CARs (Rodriguez *et al.*, 2014; Diaz *et al.*, 2016). We
521 envision that RALF1 may promote the rapid accumulation of CAR proteins to induce
522 membrane curvature and the nano-organization of the plasma membrane. Furthermore,
523 we found that FER-dependent phosphorylation of CARs, which occurs in the proximity
524 of conserved Asp residues involved in Ca^{2+} binding (Diaz *et al.*, 2016), seems to impair
525 CAR binding to vesicles. Therefore, in the first minutes following RALF1 perception
526 (<10 min), FER stimulates CAR proteins accumulation by upregulating its translation
527 and might also trigger CAR membrane recruitment in a Ca^{2+} -dependent manner. In a
528 second step (>20 min), phosphorylation of specific Ser/Thr/Tyr residues in the C2
529 domain of CARs might tune CAR binding to membranes. Mechanistically, the addition
530 of negative charges within the lipid-binding pocket of the C2 domain by
531 phosphorylation might repel the interaction with negatively charged phospholipid in
532 the PM (Simon *et al.*, 2016; Platre *et al.*, 2018). Thus, the system appears to be designed
533 for a fast-self-amplified recruitment of CAR in PM, followed by a brake mechanism
534 leading to CAR membrane dissociation. This scenario becomes even more complex
535 when considering that RALF1-FER signaling is a master regulator of cell wall integrity
536 (Zhang *et al.*, 2020), and the cell wall also has profound roles in the diffusion

537 coefficients and PM compartmentalization of resident proteins (Luu *et al.*, 2012;
538 Martiniere *et al.*, 2012; McKenna *et al.*, 2019; Danek *et al.*, 2020; Jaillais & Ott, 2020).

539 A recent study unraveled the regulation of FLS2 and BAK1 nanoscale
540 organization by the RALF receptor FER (Gronnier *et al.*, 2022). How FLS2 and BAK1
541 associate in a ligand-dependent manner within the plasma membrane in response to
542 RALF peptides needs further study. Herein, we found that the receptor kinase FER
543 regulate the lipid order of the PM via CAR proteins, which may offer a strategy to
544 modulate the formation of other receptor kinase complexes (e.g., FLS2 and BAK1).
545 Various studies indicate that FER regulates many aspects of plant biology, including
546 growth, development, environmental adaptability, and immunity, by sensing a variety
547 of external signals (Zhang *et al.*, 2020; Zhu *et al.*, 2021). Similarly, we also found a
548 pleiotropic phenotype in the high-order CAR mutants (Rodriguez *et al.*, 2014),
549 indicating that CAR-mediated regulation of membrane order could be pivotal for
550 additional signaling systems.

551 Interesting future research topics include whether RALF1–FER regulates various
552 cell type–specific outputs and/or signaling events via the dynamic nanoclustering of
553 proteins and lipids (involving other receptor kinase complexes, ROPs, CARs and
554 phosphatidylserine) of the PM. More studies are also needed to verify whether signal–
555 triggered PM compartmentalization based on kinase receptors and C2 domain–
556 containing proteins is a common mechanism in eukaryotic cells. In addition, previous
557 evidence indicates that CAR proteins are located not only in the PM but also in the
558 cytoplasm and nucleus, where these proteins participate in ABA signaling (Rodriguez
559 *et al.*, 2014) and interact with LOT1 to enhance plant drought tolerance (Qin *et al.*,
560 2019). It would be interested to address whether the RALF1-mediated regulation of
561 CAR accumulation, its membrane interaction dynamics, and its phosphorylation may
562 also impact ABA signaling.

563 **Data availability**

564 The authors declare that the data supporting the findings of this study are available
565 within the paper and its supplementary information.

566 **Acknowledgments**

567 We thank Liming Xiong, Tao Qin, and Chao Li for providing plant materials and Cyril
568 Zipfel for critical comments and suggestions. This work was supported by grants from
569 National Natural Science Foundation of China (NSFC–31871396, 31571444), China
570 Postdoctoral Science Foundation funded project (2020M672475), and the Science and
571 Technology Innovation Program of Hunan Province (2021JJ40060) to F.X. Work in
572 P.L.R. laboratory was supported by grant PID2020-113100RB funded by MCIN/AEI/
573 10.13039/501100011033.

574 **Author contributions**

575 F.Y., and W.C. conceived the project and designed the research; W.C., H.Z., S.Z., F.X.,
576 M.Y., G.X., J.C. A.C., L.R., Y.L, Q.X., and Q.F performed the research; D.W., X.L.,
577 A.C., X.L, and P.L.R. contributed new reagents/analytic tools; F.Y. and W.C. analyzed
578 data and wrote the paper with contribution from P.L.R. and Y. J.; all authors reviewed
579 and approved the manuscript for publication.

580 **Conflicts of interest**

581 The authors declare no competing financial interests.

582 **References**

- 583 **Bucherl CA, Jarsch IK, Schudoma C, Segonzac C, Mbengue M, Robatzek S, MacLean D, Ott T,**
584 **Zipfel C. 2017.** Plant immune and growth receptors share common signalling components but
585 localise to distinct plasma membrane nanodomains. *Elife* **6**.
- 586 **Burkart RC, Stahl Y. 2017.** Dynamic complexity: plant receptor complexes at the plasma membrane.
587 *Curr Opin Plant Biol* **40**: 15-21.
- 588 **Chen GH, Liu MJ, Xiong Y, Sheen J, Wu SH. 2018.** TOR and RPS6 transmit light signals to enhance
589 protein translation in deetirolating Arabidopsis seedlings. *Proc Natl Acad Sci U S A* **115**(50):
590 12823-12828.
- 591 **Chen J, Yu F, Liu Y, Du C, Li X, Zhu S, Wang X, Lan W, Rodriguez PL, Liu X, et al. 2016.** FERONIA
592 interacts with ABI2-type phosphatases to facilitate signaling cross-talk between abscisic acid

593 and RALF peptide in Arabidopsis. *Proc Natl Acad Sci U S A* **113**(37): E5519-5527.

594 **Danek M, Angelini J, Malinska K, Andrejch J, Amlerova Z, Kocourkova D, Brouzdova J,**
595 **Valentova O, Martinec J, Petrasek J. 2020.** Cell wall contributes to the stability of plasma
596 membrane nanodomain organization of Arabidopsis thaliana FLOTILLIN2 and
597 HYPERSENSITIVE INDUCED REACTION1 proteins. *Plant J* **101**(3): 619-636.

598 **Demir F, Horntrich C, Blachutzik JO, Scherzer S, Reinders Y, Kierszniowska S, Schulze WX,**
599 **Harms GS, Hedrich R, Geiger D. 2013.** Arabidopsis nanodomain-delimited ABA signaling
600 pathway regulates the anion channel SLAH3. *Proc Natl Acad Sci U S A* **110**(20): 8296-8301.

601 **Diaz M, Sanchez-Barrena MJ, Gonzalez-Rubio JM, Rodriguez L, Fernandez D, Antoni R, Yunta**
602 **C, Belda-Palazon B, Gonzalez-Guzman M, Peirats-Llobet M, et al. 2016.** Calcium-
603 dependent oligomerization of CAR proteins at cell membrane modulates ABA signaling. *Proc*
604 *Natl Acad Sci U S A* **113**(3): E396-405.

605 **Du C, Li X, Chen J, Chen W, Li B, Li C, Wang L, Li J, Zhao X, Lin J. 2016.** Receptor kinase complex
606 transmits RALF peptide signal to inhibit root growth in Arabidopsis. *Proc Natl Acad Sci U S A*
607 **113**(51): E8326-E8334.

608 **Du C, Li X, Chen J, Chen W, Li B, Li C, Wang L, Li J, Zhao X, Lin J, et al. 2016.** Receptor kinase
609 complex transmits RALF peptide signal to inhibit root growth in Arabidopsis. *Proc Natl Acad*
610 *Sci U S A* **113**(51): E8326-E8334.

611 **Duan Q, Kita D, Li C, Cheung AY, Wu H-M. 2010.** FERONIA receptor-like kinase regulates RHO
612 GTPase signaling of root hair development. *Proc Natl Acad Sci U S A* **107**(41): 17821-17826.

613 **Escobar-Restrepo JM, Huck N, Kessler S, Gagliardini V, Gheyselinck J, Yang WC, Grossniklaus**
614 **U. 2007.** The FERONIA receptor-like kinase mediates male-female interactions during pollen
615 tube reception. *science* **317**(5838): 656-660.

616 **Garcia-Parajo MF, Cambi A, Torreno-Pina JA, Thompson N, Jacobson K. 2014.** Nanoclustering as
617 a dominant feature of plasma membrane organization. *J Cell Sci* **127**(Pt 23): 4995-5005.

618 **Gronnier J, Franck CM, Stegmann M, DeFalco TA, Abarca A, Von Arx M, Dünser K, Lin W, Yang**
619 **Z, Kleine-Vehn J, et al. 2022.** Regulation of immune receptor kinase plasma membrane
620 nanoscale organization by a plant peptide hormone and its receptors. *Elife* **11**.

621 **Guo H, Li L, Ye H, Yu X, Algreen A, Yin Y. 2009.** Three related receptor-like kinases are required for
622 optimal cell elongation in Arabidopsis thaliana. *Proc Natl Acad Sci U S A* **106**(18): 7648-7653.

623 **Huang D, Sun Y, Ma Z, Ke M, Cui Y, Chen Z, Chen C, Ji C, Tran TM, Yang L, et al. 2019.** Salicylic
624 acid-mediated plasmodesmal closure via Remorin-dependent lipid organization. *Proc Natl Acad*
625 *Sci U S A* **116**(42): 21274-21284.

626 **Jaillais Y, Ott T. 2020.** The Nanoscale Organization of the Plasma Membrane and Its Importance in
627 Signaling: A Proteolipid Perspective. *Plant Physiol* **182**(4): 1682-1696.

628 **James J, Fiji N, Roy D, Andrew Mg D, Shihabudeen MS, Chattopadhyay D, Thirumurugan K.**
629 **2015.** A rapid method to assess reactive oxygen species in yeast using H2DCF-DA. *Analytical*
630 *Methods* **7**(20): 8572-8575.

631 **Jarsch IK, Konrad SS, Stratil TF, Urbanus SL, Szymanski W, Braun P, Braun KH, Ott T. 2014.**
632 Plasma Membranes Are Subcompartmentalized into a Plethora of Coexisting and Diverse
633 Microdomains in Arabidopsis and Nicotiana benthamiana. *Plant Cell* **26**(4): 1698-1711.

634 **Larsen JB, Jensen MB, Bhatia VK, Pedersen SL, Bjørnholm T, Iversen L, Uline M, Szleifer I,**
635 **Jensen KJ, Hatzakis NS. 2015.** Membrane curvature enables N-Ras lipid anchor sorting to
636 liquid-ordered membrane phases. *Nature chemical biology* **11**(3): 192.

637 **Li C, Liu X, Qiang X, Li X, Zhu S, Wang L, Wang Y, Liao H, Luan S, Yu F. 2018.** EBP1 nuclear
638 accumulation negatively feeds back on FERONIA-mediated RALF1 signaling. *PLoS Biol*
639 **16(10): e2006340.**

640 **Li C, Yeh F-L, Cheung AY, Duan Q, Kita D, Liu M-C, Maman J, Luu EJ, Wu BW, Gates L. 2015.**
641 Glycosylphosphatidylinositol-anchored proteins as chaperones and co-receptors for FERONIA
642 receptor kinase signaling in Arabidopsis. *Elife* **4: e06587.**

643 **Liang P, Stratil TF, Popp C, Marin M, Folgmann J, Mysore KS, Wen J, Ott T. 2018.** Symbiotic root
644 infections in *Medicago truncatula* require remorin-mediated receptor stabilization in membrane
645 nanodomains. *Proc Natl Acad Sci U S A* **115(20): 5289-5294.**

646 **Luu DT, Martiniere A, Sorieul M, Runions J, Maurel C. 2012.** Fluorescence recovery after
647 photobleaching reveals high cycling dynamics of plasma membrane aquaporins in Arabidopsis
648 roots under salt stress. *Plant J* **69(5): 894-905.**

649 **Martens S, Kozlov MM, McMahan HT. 2007.** How synaptotagmin promotes membrane fusion.
650 *science* **316(5828): 1205-1208.**

651 **Martens S, McMahan HT. 2008.** Mechanisms of membrane fusion: disparate players and common
652 principles. *Nat Rev Mol Cell Biol* **9(7): 543-556.**

653 **Martiniere A, Lavagi I, Nageswaran G, Rolfe DJ, Maneta-Peyret L, Luu DT, Botchway SW, Webb
654 SED, Mongrand S, Maurel C, et al. 2012.** Cell wall constrains lateral diffusion of plant
655 plasma-membrane proteins. *Proc Natl Acad Sci U S A* **109(31): 12805-12810.**

656 **McKenna JF, Rolfe DJ, Webb SED, Tolmie AF, Botchway SW, Martin-Fernandez ML, Hawes C,
657 Runions J. 2019.** The cell wall regulates dynamics and size of plasma-membrane nanodomains
658 in Arabidopsis. *Proc Natl Acad Sci U S A* **116(26): 12857-12862.**

659 **Missra A, Von Arnim AG. 2014.** Analysis of mRNA Translation States in Arabidopsis Over the Diurnal
660 Cycle by Polysome Microarray. *Methods of Molecular Biology* **1158: 157-174.**

661 **Ngo QA, Vogler H, Lituiev D, Nestorova A, Grossniklaus UJDC. 2014.** A calcium dialog mediated
662 by the FERONIA Signal transduction pathway controls plant sperm delivery. *Developmental
663 Cell* **29(4): 491-500.**

664 **Ott T. 2017.** Membrane nanodomains and microdomains in plant-microbe interactions. *Curr Opin Plant
665 Biol* **40: 82-88.**

666 **Owen DM, Rentero C, Magenau A, Abu-Siniyeh A, Gaus K. 2011.** Quantitative imaging of membrane
667 lipid order in cells and organisms. *Nat Protoc* **7(1): 24-35.**

668 **Pan X, Fang L, Liu J, Senay-Aras B, Lin W, Zheng S, Zhang T, Guo J, Manor U, Van Norman J,
669 et al. 2020.** Auxin-induced signaling protein nanoclustering contributes to cell polarity
670 formation. *Nat Commun* **11(1): 3914.**

671 **Platre MP, Bayle V, Armengot L, Bareille J, Marquès-Bueno MdM, Creff A, Maneta-Peyret L,
672 Fiche J-B, Nollmann M, Miège C, et al. 2019.** Developmental control of plant Rho GTPase
673 nano-organization by the lipid phosphatidylserine. *science* **364(6435): 57-62.**

674 **Platre MP, Noack LC, Doumane M, Bayle V, Simon MLA, Maneta-Peyret L, Fouillen L, Stanislas
675 T, Armengot L, Pejchar P, et al. 2018.** A Combinatorial Lipid Code Shapes the Electrostatic
676 Landscape of Plant Endomembranes. *Dev Cell* **45(4): 465-480 e411.**

677 **Qin T, Tian Q, Wang G, Xiong L. 2019.** LOWER TEMPERATURE 1 Enhances ABA Responses and
678 Plant Drought Tolerance by Modulating the Stability and Localization of C2-Domain ABA-
679 Related Proteins in Arabidopsis. *Mol Plant* **12(9): 1243-1258.**

680 **Rodriguez L, Gonzalez-Guzman M, Diaz M, Rodrigues A, Izquierdo-Garcia AC, Peirats-Llobet M,**

681 **Fernandez MA, Antoni R, Fernandez D, Marquez JA, et al. 2014.** C2-domain abscisic acid-
682 related proteins mediate the interaction of PYR/PYL/RCAR abscisic acid receptors with the
683 plasma membrane and regulate abscisic acid sensitivity in Arabidopsis. *Plant Cell* **26**(12): 4802-
684 4820.

685 **Sezgin E, Levental I, Mayor S, Eggeling C. 2017.** The mystery of membrane organization: composition,
686 regulation and roles of lipid rafts. *Nat Rev Mol Cell Biol* **18**(6): 361-374.

687 **Simon ML, Platre MP, Marques-Bueno MM, Armengot L, Stanislas T, Bayle V, Caillaud MC,
688 Jaillais Y. 2016.** A PtdIns(4)P-driven electrostatic field controls cell membrane identity and
689 signalling in plants. *Nat Plants* **2**: 16089.

690 **Simons K, Gerl MJ. 2010.** Revitalizing membrane rafts: new tools and insights. *Nature Reviews*
691 *Molecular Cell Biology* **11**(10): 688-699.

692 **Spira F, Mueller NS, Beck G, von Olshausen P, Beig J, Wedlich-Soldner R. 2012.** Patchwork
693 organization of the yeast plasma membrane into numerous coexisting domains. *Nat Cell Biol*
694 **14**(6): 640-648.

695 **Stegmann M, Monaghan J, Smakowska-Luzan E, Rovenich H, Lehner A, Holton N, Belkhadir Y,
696 Zipfel C. 2017.** The receptor kinase FER is a RALF-regulated scaffold controlling plant
697 immune signaling. *science* **355**(6322): 287-289.

698 **Wang L, Li H, Lv X, Chen T, Li R, Xue Y, Jiang J, Jin B, Baluska F, Samaj J, et al. 2015.**
699 Spatiotemporal Dynamics of the BRI1 Receptor and its Regulation by Membrane
700 Microdomains in Living Arabidopsis Cells. *Mol Plant* **8**(9): 1334-1349.

701 **Wang L, Yang T, Wang B, Lin Q, Zhu S, Li C, Ma Y, Tang J, Xing J, Li X, et al. 2020.** RALF1-
702 FERONIA complex affects splicing dynamics to modulate stress responses and growth in plants.
703 *Sci Adv* **6**(21): eaaz1622.

704 **Xu G, Chen W, Song L, Chen Q, Zhang H, Liao H, Zhao G, Lin F, Zhou H, Yu F. 2019.** FERONIA
705 phosphorylates E3 ubiquitin ligase ATL6 to modulate the stability of 14-3-3 proteins in response
706 to the carbon/nitrogen ratio. *J Exp Bot* **70**(21): 6375-6388.

707 **Yang T, Wang L, Li C, Liu Y, Zhu S, Qi Y, Liu X, Lin Q, Luan S, Yu F. 2015.** Receptor protein kinase
708 FERONIA controls leaf starch accumulation by interacting with glyceraldehyde-3-phosphate
709 dehydrogenase. *Biochemical and biophysical research communications* **465**(1): 77-82.

710 **Zhang X, Yang Z, Wu D, Yu F. 2020.** RALF-FERONIA Signaling: Linking Plant Immune Response
711 with Cell Growth. *Plant Communications* **1**(4).

712 **Zhou YB, Liu C, Tang DY, Yan L, Wang D, Yang YZ, Gui JS, Zhao XY, Li LG, Tang XD, et al.
713 2018.** The Receptor-Like Cytoplasmic Kinase STRK1 Phosphorylates and Activates CatC,
714 Thereby Regulating H₂O₂ Homeostasis and Improving Salt Tolerance in Rice. *Plant Cell* **30**(5):
715 1100-1118.

716 **Zhu S, Estévez JM, Liao H, Zhu Y, Yang T, Li C, Wang Y, Li L, Liu X, Pacheco JM. 2020.** The
717 RALF1-FERONIA complex phosphorylates eIF4E1 to promote protein synthesis and polar root
718 hair growth. *Mol Plant* **13**: 698-716.

719 **Zhu S, Fu Q, Xu F, Zheng H, Yu F. 2021.** New paradigms in cell adaptation: decades of discoveries on
720 the CrRLK1L receptor kinase signalling network. *New Phytol* **232**(3): 1168-1183.

721 **Figures and legends**

722 **Fig. 1 FER physically interacts with CARs.**

723 (a) Y2H assays showing the interaction between CARs and FER. SD (–His/–Leu/–Trp)
724 selection medium containing 20 mM 3–AT was used to test the interaction. The CAR
725 members were cloned into the pGADT7 (AD) vector, and the FER-CD was cloned into
726 the pGBKT7 (BD) vector.

727 (b) GST pull–down assay. The indicated GST–tag and His–tag were detected by anti–
728 GST and anti–His, respectively.

729 (c) FER interacts with CARs in BiFC assays in Arabidopsis protoplasts. Negative
730 control (cCFP + FER–Venus) are shown, and FM4–64 indicates the PM (red).

731 (d) Co–IP assays. The immunoprecipitated CAR9 and coimmunoprecipitated FER were
732 indicated using anti–FER and anti–Myc antibodies, respectively.

733 At least three biological replicates of (a) – (d) were performed with similar results.

734 **Fig. 2 RALF1–FER phosphorylates CAR proteins and further regulates the**
735 **interaction of CAR proteins and lipid.**

736 (a) *In vitro* phosphorylation assays showing that FER–CD can phosphorylate GST–
737 CAR5 and GST–CAR9 are detected using anti–pSer/Thr, and anti–GST and anti–His.

738 (b) Phostag–PAGE assays *in vivo*. Phosphorylated CAR5–Myc and CAR9–Myc bands
739 are indicated as pCAR5–Myc and pCAR9–Myc.

740 (c) Examples of phosphopeptides of CAR5 *in vivo*. The maximum probability shown
741 for each phosphorylation site was calculated by the Andromeda algorithm integrated in
742 MaxQuant.

743 (d) *In vitro* phosphorylation assays showing that GST–CAR5^{3M} and GST–CAR9^{3M}
744 were not phosphorylated by FER–CD.

745 (e) GST pull–down assay showing that phosphorylated FER–CD exhibits a higher
746 affinity towards GST–CAR9^{3M}. The relative protein intensity of FER–CD–His and
747 FER^{K565R}–CD–His in the output was analyzed using ImageJ.

748 (f) GST pull–down assay. GST–CAR9^{3D} shows a weaker interaction with FER–CD–
749 His and FER^{K565R}–CD–His. The relative protein intensity of FER–CD–His and
750 FER^{K565R}–CD–His in the output was analyzed using ImageJ. The red arrow pointing

751 the weakened anti-His panel.

752 (g-h) Phosphorylated CAR5 and CAR9 (0.1 μ M) show weaker lipid binding ability in
753 the presence of 1 mM CaCl₂.

754 (i) Lipid binding abilities of three forms of CAR9 in the presence or absence of 1 mM
755 CaCl₂. Immunoblot assays showing the protein levels by ImageJ.

756 At least three biological replicates of (a) – (i) were performed with similar results.

757 **Fig. 3 RALF1-FER promotes the formation of CAR-nanoclustering by enhancing**
758 **their translation rate.**

759 (a) VA-TIRFM images of YFP-CAR9 at the PM in root cells with or without RALF1
760 (1 μ M, 10 min) or M β CD (10 mM, 30 min) treatment in WT and *fer-4* background.

761 (b) Quantitative comparison of YFP-CAR9 particle density in different groups.

762 (c) Comparison of diffusion coefficients of YFP-CAR9 particles in different groups.

763 (d) RALF1-induced accumulation of CAR proteins in WT and *fer-4*. CAR proteins
764 were detected by pan-anti-CARs antibody (see Methods for details of this antibody).

765 The relative accumulation of CAR proteins was analyzed using ImageJ.

766 (e-f) Upper panel: ribosome profiles. Fractions (8–11) containing mRNAs associated
767 with polysomes are indicated with a black line. Lower panels: RT-qPCR results of
768 polysome-associated CAR mRNAs.

769 At least three biological replicates were performed with similar results. Data are shown
770 as the mean \pm s.d., *** $p < 0.001$, n.s., not significant. One-way ANOVA with Tukey's
771 test.

772 **Fig. 4 RALF-FER module regulates the formation of ordered lipid nanodomains**
773 **through CAR proteins.**

774 (a) Di-4-ANEPPDHQ lipid staining assay of WT and *fer-4* root cells with or without
775 RALF1 treatment. The GP value is indicated with a colored box. The white triangles
776 indicate the regions for GP value quantification.

777 (b) Statistical analysis of the GP value in (a). The white triangle in (a) indicates the
778 regions for GP value quantification. For each treatment, 42 – 54 cells from 5 roots were
779 measured.

780 (c) Di-4-ANEPPDHQ lipid staining assay of WT root cells with or without M β CD and
781 RALF1 treatments. The GP value is indicated with a colored box. The white triangles
782 indicate the regions for GP value quantification.

783 (d) Statistical analysis of the GP value in (c). The white triangle in (c) indicates the
784 regions for GP value quantification. For each treatment, 42 – 54 cells from 5 roots were
785 measured.

786 (e) Di-4-ANEPPDHQ lipid staining assay in root cells of WT, *car59*, *car459*, *car1459*
787 and *car14569*- Δ 20 with or without RALF1 treatment. The GP value is indicated with
788 a colored box.

789 (f) Statistical analysis of the GP value in (e). The white triangle in (e) indicates the
790 regions for GP value quantification. For each treatment, 41 – 60 cells from 5 roots were
791 measured.

792 All experiments were replicated three times with similar results. Data are shown as the
793 mean \pm s.d.; **p* < 0.05, ***p* < 0.01, ****p* < 0.001, n.s., not significant. One-way
794 ANOVA with Tukey's test.

795 **Fig. 5 RALF1-FER-CAR axis as a signaling platform to integrate immunity**
796 **response.**

797 (a-b) Co-IP assay showing the weaker interaction between FLS2 and BAK1 in *fer-4*
798 and *car14569*- Δ 20 with or without RALF1 and flg22 treatment for 10 min. Western
799 blots were probed with anti-FLS2 and anti-BAK1 antibodies. The relative protein
800 intensity of FLS2 and BAK1 was analyzed using Image J.

801 (c) Quantitative comparison of FLS2 and BAK1 interaction strength in (a) and (b). The
802 ratio of BAK1 to FLS2 in (a) and (b) were normalized.

803 (d-e) The ROS burst was measured after elicitation of leaf discs from the indicated
804 mutant lines with 0.1 μ M flg22 and/or 1 μ M RALF1 in (d). (e) was showed the ROS
805 integration as mean values of total photon counts over 1500 second in (d).

806 (f) Colony-forming units (cfu) of *Pto* DC3000 bacteria after infection for 3 days.

807 (g) Bacterial populations statistics after infection for 3 days. Bacterial inoculations were
808 performed as described in (f). Log_{10} CFU/cm², log_{10} colony-forming units per cm² of
809 leaf tissue.

810 All experiments were replicated three times with similar results. Data are shown as the
811 mean \pm s.d.; *** $p < 0.001$, n.s., not significant. One-way ANOVA with Tukey's test.

812 **Fig. 6 A working model for RALF1-dependent plant response through the FER-**
813 **CAR axis in the formation of proper lipid ordered nanodomains**

814 The RALF1–FER signaling first promotes CAR protein synthesis, and then, more CAR
815 proteins localize to the PM via binding Ca^{2+} and interacting with negative charge
816 phospholipids, which positively regulates formation of lipid ordered nanodomains and
817 membrane curvature. Finally, FER interacts with and phosphorylates CARs in a
818 RALF1–dependent manner. The enhanced phosphorylation level of CARs reduces their
819 binding to negatively charged phospholipids. This maintains the dynamic balance of
820 CAR proteins on the membrane, thus, serving for fine-tuning of the system sensitivity.
821 Proteins and structures are not to scale.

822 **Supporting Information**

823 **Fig. S1** FER physically interacts with CARs.

824 **Fig. S2** Phostag–PAGE analysis dynamics of CAR5 and CAR9 protein phosphorylation.

825 **Fig. S3** ESI mass spectrometry identification of CARs phosphorylation sites.

826 **Fig. S4** Functional analysis of CAR protein phosphorylation sites.

827 **Fig. S5** CAR proteins directly interact with anionic lipids and promote lipid tubules.

828 **Fig. S6** The effect of phosphorylation on the dwell time of CAR9 in nanodomain.

829 **Fig. S7** RALF1 induces CARs protein accumulation.

830 **Fig. S8** CAR9 partially rescued the lipid order of *fer-4*.

831 **Fig. S9** RALF1 induces the formation of lipid ordering through rapid accumulation of CAR proteins.

832 **Fig. S10** Lipid order nanodomains are crucial for plant immunity.

833 **Fig. S11** The nanocluster of CAR9 is insensitive to *flg22* treatment.

834 **Fig. S12** FER-CAR module is crucial for immune response.

835 **Fig. S13** *fer-4* and multiple CAR mutants phenotype analysis.

836

837 **Table S1** Primers used in this study.

838 **Methods S1** Detailed Methods Description

Figures and legends

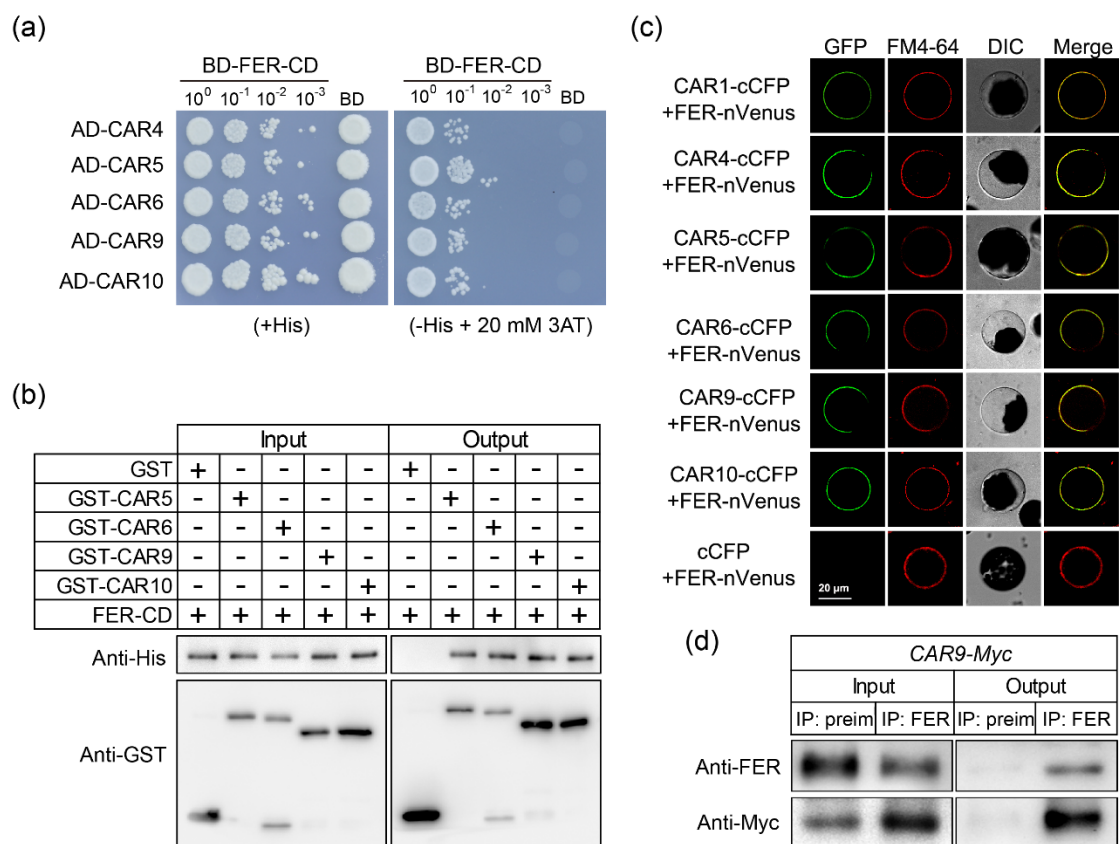


Fig. 1 FER physically interacts with CARs.

(a) Y2H assays showing the interaction between CARs and FER. SD (-His/-Leu/-Trp) selection medium containing 20 mM 3-AT was used to test the interaction. The CAR members were cloned into the pGADT7 (AD) vector, and the FER-CD was cloned into the pGBKT7 (BD) vector.

(b) GST pull-down assay. The indicated GST-tag and His-tag were detected by anti-GST and anti-His, respectively.

(c) FER interacts with CARs in BiFC assays in Arabidopsis protoplasts. Negative control (cCFP + FER-Venus) are shown, and FM4-64 indicates the PM (red).

(d) Co-IP assays. The immunoprecipitated CAR9 and coimmunoprecipitated FER were indicated using anti-FER and anti-Myc antibodies, respectively.

At least three biological replicates of (a) – (d) were performed with similar results.

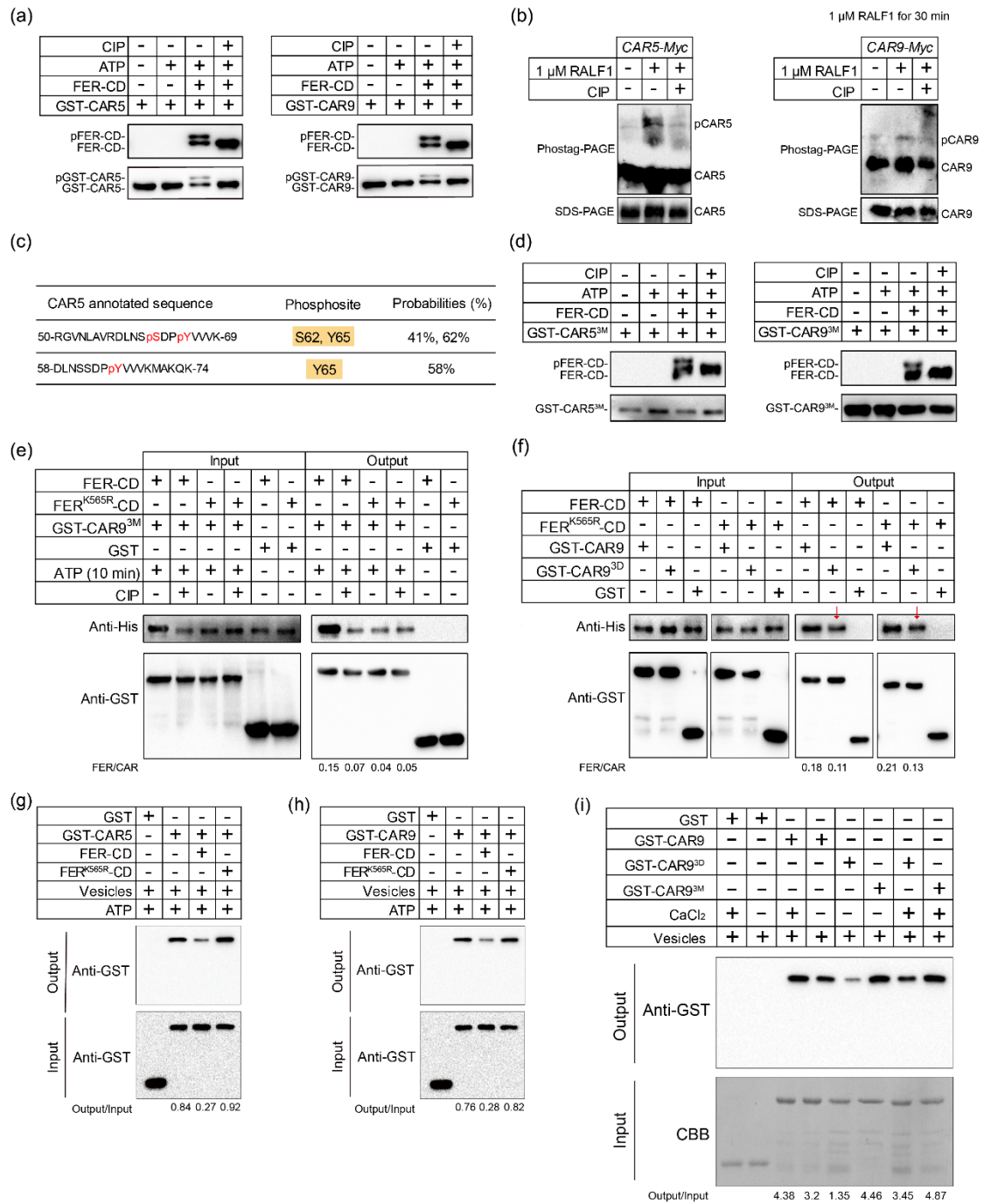


Fig. 2 RALF1-FER phosphorylates CAR proteins and further regulates the interaction of CAR proteins and lipids.

(a) *In vitro* phosphorylation assays showing that FER-CD can phosphorylate GST-CAR5 and GST-CAR9 are detected using anti-pSer/Thr, and anti-GST and anti-His.

(b) Phostag-PAGE assays *in vivo*. Phosphorylated CAR5-Myc and CAR9-Myc bands are indicated as pCAR5-Myc and pCAR9-Myc.

(c) Examples of phosphopeptides of CAR5 *in vivo*. The maximum probability shown for each phosphorylation site was calculated by the Andromeda algorithm integrated in

MaxQuant.

(d) *In vitro* phosphorylation assays showing that GST-CAR5^{3M} and GST-CAR9^{3M} were not phosphorylated by FER-CD.

(e) GST pull-down assay showing that phosphorylated FER-CD exhibits a higher affinity towards GST-CAR9^{3M}. The relative protein intensity of FER-CD-His and FER^{K565R}-CD-His in the output was analyzed using ImageJ.

(f) GST pull-down assay. GST-CAR9^{3D} shows a weaker interaction with FER-CD-His and FER^{K565R}-CD-His. The relative protein intensity of FER-CD-His and FER^{K565R}-CD-His in the output was analyzed using ImageJ. The red arrow pointing the weakened anti-His panel.

(g-h) Phosphorylated CAR5 and CAR9 (0.1 μ M) show weaker lipid binding ability in the presence of 1 mM CaCl₂.

(i) Lipid binding abilities of three forms of CAR9 in the presence or absence of 1 mM CaCl₂. Immunoblot assays showing the protein levels by ImageJ.

At least three biological replicates of (a) – (i) were performed with similar results.

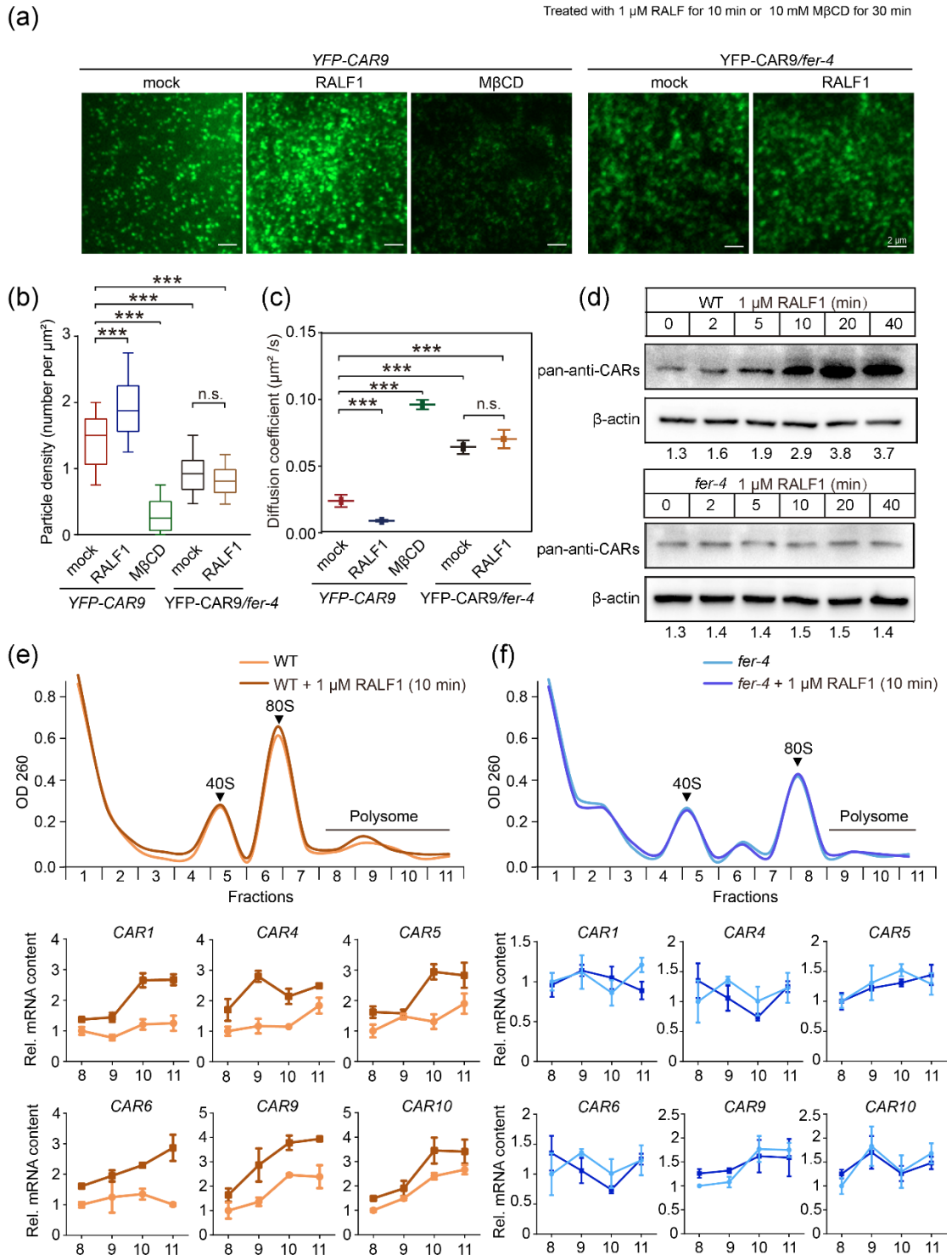


Fig. 3 RALF1-FER promotes the formation of CAR-nanoclustering by enhancing their translation rate.

- (a) VA-TIRFM images of YFP-CAR9 at the PM in root cells with or without RALF1 (1 μ M, 10 min) or M β CD (10 mM, 30 min) treatment in WT and *fer-4* background.
- (b) Quantitative comparison of YFP-CAR9 particle density in different groups.
- (c) Comparison of diffusion coefficients of YFP-CAR9 particles in different groups.

(d) RALF1-induced accumulation of CAR proteins in WT and *fer-4*. CAR proteins were detected by pan-anti-CARs antibody (see Methods for details of this antibody). The relative accumulation of CAR proteins was analyzed using ImageJ.

(e-f) Upper panel: ribosome profiles. Fractions (8–11) containing mRNAs associated with polysomes are indicated with a black line. Lower panels: RT-qPCR results of polysome-associated CAR mRNAs.

At least three biological replicates were performed with similar results. Data are shown as the mean \pm s.d., *** $p < 0.001$, n.s., not significant. One-way ANOVA with Tukey's test.

+ 1 μ M RALF1, 10 min; 10 mM M β CD, 30 min

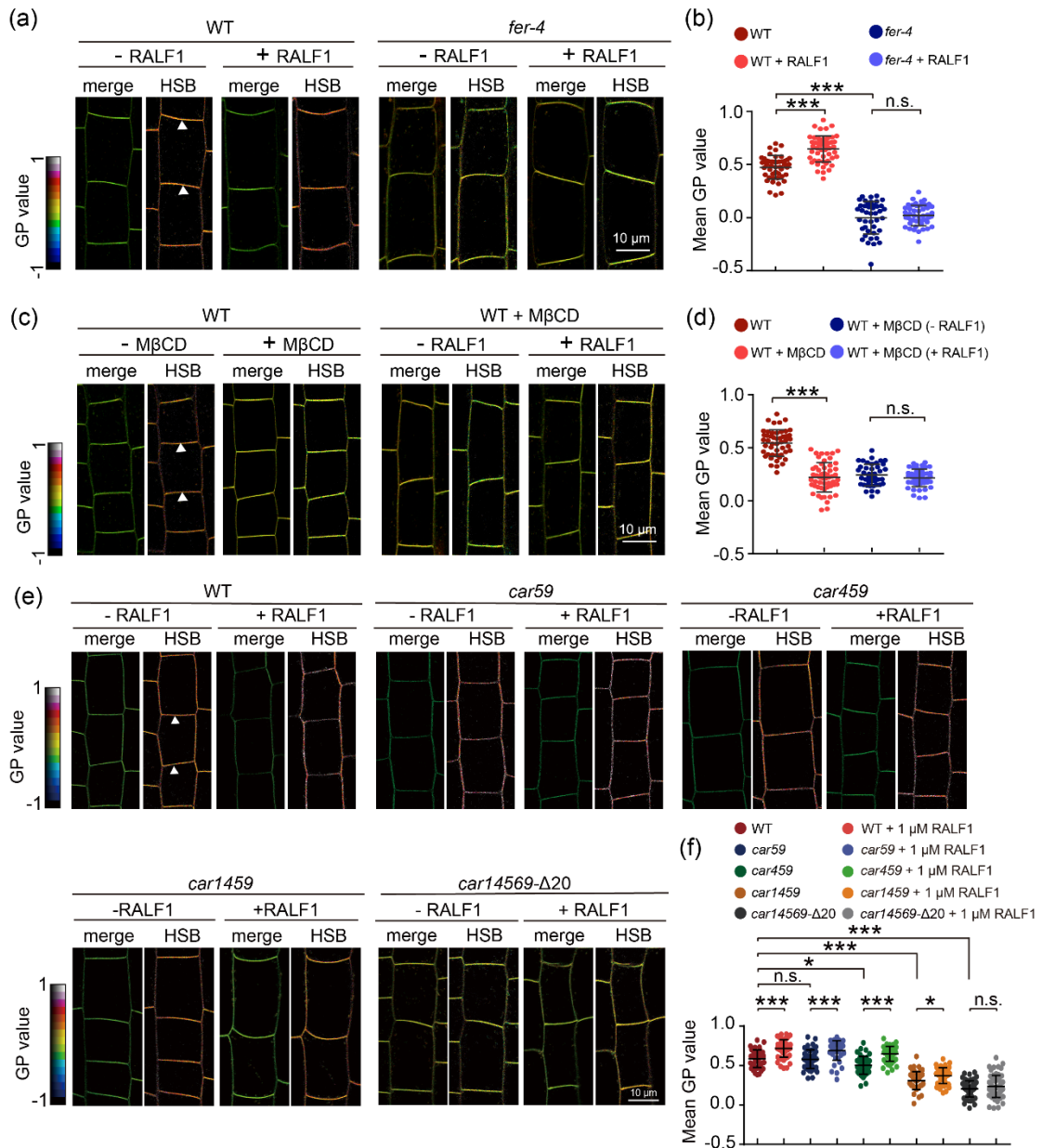


Fig. 4 RALF-FER module regulates the lipid order of the plasma membrane through CAR proteins.

(a) Di-4-ANEPPDHQ lipid staining assay of WT and *fer-4* root cells with or without RALF1 treatment. The GP value is indicated with a colored box. The white triangles indicate the regions for GP value quantification.

(b) Statistical analysis of the GP value in (a). The white triangle in (a) indicates the regions for GP value quantification. For each treatment, 42 – 54 cells from 5 roots were measured.

(c) Di-4-ANEPPDHQ lipid staining assay of WT root cells with or without M β CD and RALF1 treatments. The GP value is indicated with a colored box. The white triangles indicate the regions for GP value quantification.

(d) Statistical analysis of the GP value in (c). The white triangle in (c) indicates the regions for GP value quantification. For each treatment, 42 – 54 cells from 5 roots were measured.

(e) Di-4-ANEPPDHQ lipid staining assay in root cells of WT, *car59*, *car459*, *car1459* and *car14569*- Δ 20 with or without RALF1 treatment. The GP value is indicated with a colored box.

(f) Statistical analysis of the GP value in (e). The white triangle in (e) indicates the regions for GP value quantification. For each treatment, 41 – 60 cells from 5 roots were measured.

All experiments were replicated three times with similar results. Data are shown as the mean \pm s.d.; *p < 0.05, **p < 0.01, ***p < 0.001, n.s., not significant. One-way ANOVA with Tukey's test.

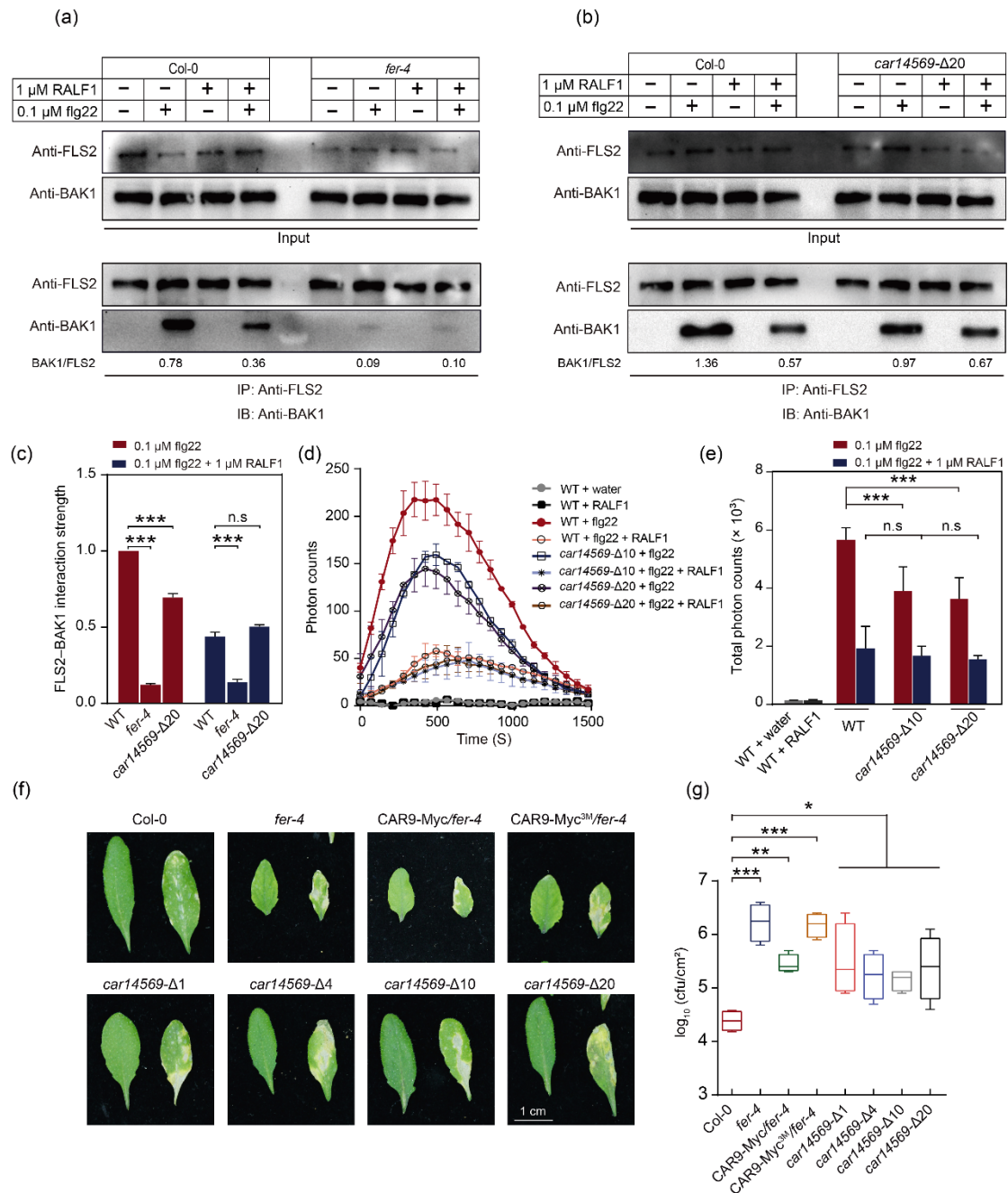


Fig. 5 The RALF1-FER-CAR axis as a signaling platform to integrate immunity response.

(a-b) Co-IP assay showing the weaker interaction between FLS2 and BAK1 in *fer-4* and *car14569-Δ20* with or without RALF1 and flg22 treatment for 10 min. Western blots were probed with anti-FLS2 and anti-BAK1 antibodies. The relative protein intensity of FLS2 and BAK1 was analyzed using Image J.

(c) Quantitative comparison of FLS2 and BAK1 interaction strength in (a) and (b). The ratio of BAK1 to FLS2 in (a) and (b) were normalized.

(d-e) The ROS burst was measured after elicitation of leaf discs from the indicated mutant lines with 0.1 μM flg22 and/or 1 μM RALF1 in (d). (e) was showed the ROS integration as mean values of total photon counts over 1500 second in (d).

(f) Colony-forming units (cfu) of *Pto* DC3000 bacteria after infection for 3 days.

(g) Bacterial populations statistics after infection for 3 days. Bacterial inoculations were performed as described in (f). Log_{10} CFU/cm², log_{10} colony-forming units per cm² of leaf tissue.

All experiments were replicated three times with similar results. Data are shown as the mean \pm s.d.; *** $p < 0.001$, n.s., not significant. One-way ANOVA with Tukey's test.

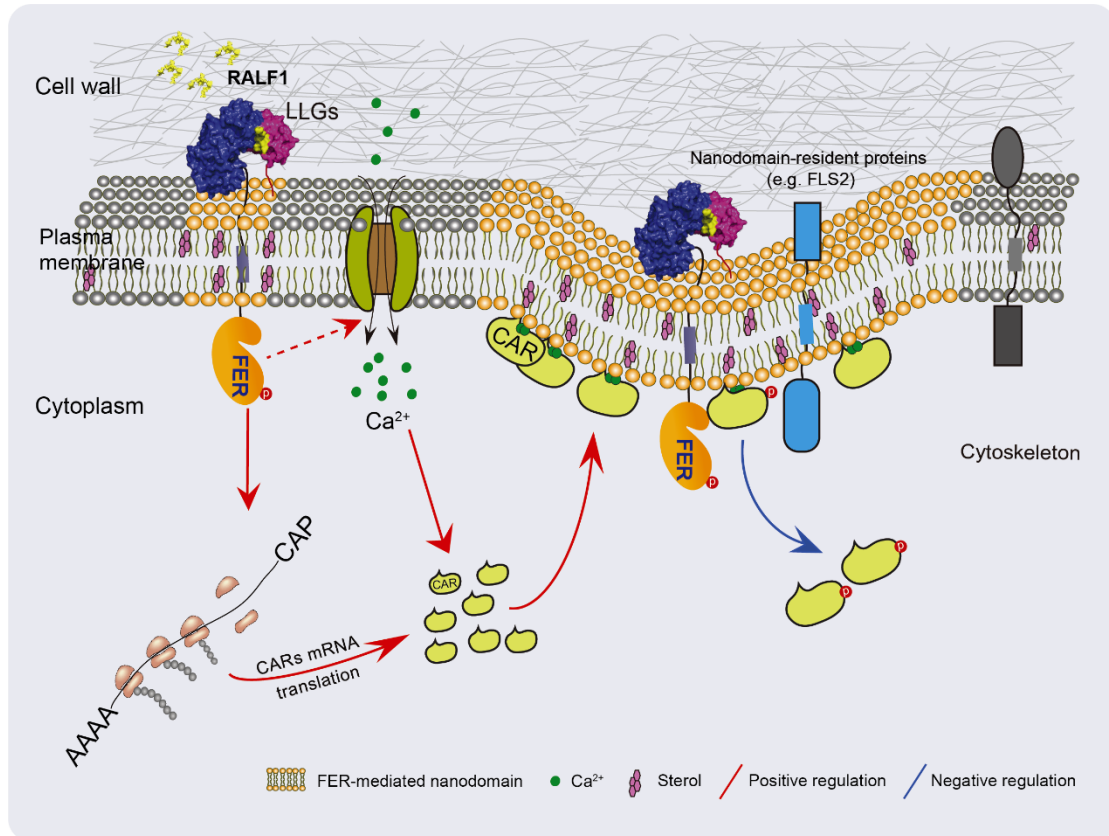


Fig. 6 A working model for RALF1-dependent plant response through the FER-CAR axis in the regulation of plasma membrane nano-organization.

The RALF1–FER signaling first promotes CAR protein synthesis. CAR proteins localize to the PM via binding Ca²⁺ and interacting with negatively charged phospholipids. At the plasma membrane, they induce membrane curvature and promote a liquid-ordered state of the plasma membrane. Finally, FER interacts with and phosphorylates CARs in a RALF1–dependent manner. The enhanced phosphorylation level of CARs reduces their binding to negatively charged phospholipids. This maintains a dynamic balance of CAR proteins on the membrane, and fine-tune the sensitivity of the system. Proteins and structures are not to scale.